ENGINEERING RESEARCH JOURNAL (ERJ)
Vol. 1, No. 51 Jan 2022, pp.43-49
Journal Homepage: erj.bu.edu.eg

A method for calibrating a single facet small heliostat based on extracting invariant moments

M. A. Abdelmagid[1], M. M.Naguib[2], A. M. Hamdy[3], A. A. El-samahy[4] and M. A. Rady[5]

[1,5] Department of Mechanical Engineering, Faculty of Engineering, Helwan, Egypt.
[3] Department of Computers Engineering and Systems, Faculty of Engineering, Helwan, Egypt.
[2,4] Department of Electrical Power and Machines Engineering, Faculty of Engineering, Helwan, Egypt.

Abstract : paper presents a new technique for calibrating heliostat errors which affect the heliostat efficiency and the production of thermal energy from the reflected beam from mirror to the target. This technique is based on analyzing the image for identifying different deterministic error types in single facet small heliostat, such as pedestal tilt and deformation due to wind loading. The technique depends on the image constructed from reflected beam. For each image, seven features are extracted and stored. These features are based on the moment invariant technique, which is insensitive to translation, rotation, and scale changes. The obtained results verify accurate and fast operation for heliostat calibration. The computed false negative rate is 0.06 and the recognition rate is 94.0476 %.

Index Terms: Image analysis, Calibration, Heliostat.

List of abbreviations

μ	Central Moment
CCD	Charge-Coupled Device
CSP	Concentrating Solar Power
De	Euclidean distance
FN	False negative
FP	False positive
FNR	False negative rate
φ_i	Invariant moments
m	Moment
η	Normalized Central Moment
PV	Photovoltaic
TPR	True positive rate

Introduction

In recent years, fossil fuels became an undesirable source of energy due to several reasons; resultant pollution, high-cost extracting, and a shortage of the fuel in certain areas in the world. For these this reasons, the world's leaders head their intention on renewable energy resources instead of fossil fuel. Wind, solar, geothermal, wave, etc. are natural sources of energy that are renewed day by day with a huge capacity that allows us to depend completely on it as a main source of power. An amount of 5.49718 x 1024 Jules of

solar energy is annually received from the sunReda and Andreas[1]. That huge amount of sustainable energy leads us to invent many types of tools to extract this energy for our daily usage. Photovoltaic(PV) and Concentrated Solar Power (CSP) are two types that produce energy from the sunlight. PV considered one of the spreading technologies that are used now as domestic products. However, we need more sustainable technology which can generate a huge amount of energy in order to supply the critical loads in our electric networks. CSP considered one of the most promising solar energy technologies in the last decades. The huge amount of energy generated from CSP plants made it a needed technology to be used. CSP gets to benefit from the sun by concentrating the sun ray's radiation using certain shapes of concentrators toward a certain target. The concentrated radiation heats up a fluid that evaporates and drive a turbine to produce electricity.

During the development and operation phases of solar power plants, the calibration of concentrating solar power (CSP) systems is an important task. During the development phase, it helps in enhancing the design of reflecting and receiving systems. However, during the operation phase, it is affecting the plant's efficiency and performance losses introduced by some errors in the tracking system. Basically, the CSP's optical performance depends on the mirror's ability to reflect accurately the sunlight on the receiver.

The heliostat calibration method is based on measuring the reflected flux on a target Pfahl et al. [2]. The flux's distribution of the reflected light is acquired by cameras and then analyzed. The acquisition process is subjected to some errors due to the sun light spot movement on the target. The acquisition is affected by different error sources, deterministic and non- deterministic errors. Deterministic errors are easily quantified and measured; e.g.; pedestal tilt, azimuth and elevation reference, deformation due to wind loading, non-level terrain, gear backlash, back drive of the heliostat and low encoder resolution.Non-deterministic errors are difficult to predict, control, and quantify indirectly. These types of errors should be eliminated prior to the system installation; e.g.; reflecting surface deformation, reflectivity reduction by aging, sensor accuracy reduction with aging and gear ratio choice.

The research work in Masters [3] proposed algorithms for detection and correction of movements of a colored model target. The proposed model has the ability of detecting movements in the tower with ±0.32 degrees' average error. An approach for tracking heliostat using image analysis and signal modulation is proposed in Bern et al.[4]. The proposed approach aimed to extract the focal spot position within the receiver. A procedure for automatic calibration using attached cameras to each heliostat is presented in Burisch et al.[5]. The cameras were monitoring different targets distributed through the solar field. A methodology for dynamic wind loading evaluation was presented in Terrés-Nícoli et al. [6]. A pressure model of 1:50 scale was examined in a boundary layer wind tunnel.

A low-cost and modular heliostat for tower-based CSP was proposed in Zavodnyaet al.[7]. Large quantities of small single-facet (∼2.2 m^2) had been achieved by individual heliostats controller. Different types of errors were presented in Freeman et al.[8]. The difficulty level of resolution was identified in heliostat based on solar energy systems.

In Younkin et al. [9], three main types of tracking and calibration controllers have been presented. In passive methods, the tracking does not depend on microcontrollers or sensors Ebrahimi[10], Ziegler[11]. This method is suitable for solar tracking PV, but it cannot provide the required accuracy in heliostat systems. In sensor-based microcontroller methods (active method), sun sensors are used for adaptive control and self-calibration of heliostats Koren[12]. Camera-based machine vision is used in large heliostat field tracking control and calibration. Closed loop control and calibration method using photodiodes and piezoelectric actuators have been introduced by Freeman[13]. The improved accuracy and robustness come at the expense of the extra cost of sensors and control system. The system also becomes more complex as the number of heliostats increases.

The present work aims to calibrate a single facet small heliostat based on extracting invariant moments withcharge-coupled device(CCD) camera. The major contribution of the present work is the design and implementation of a simple low-cost calibration system with easy installation, high precision, low maintenance, time saving and calibration without sun. The system has the ability to track the sun and correct any deviation in the tracking system. Investigation of the influences of calibration system that enables accurate individual heliostat tracking rapidly upon commissioning.

2. THE PROPOSED TECHNIQUE

In this research work, a calibration system of single facet small heliostat is proposed. The system consists of heliostat, camera, calibration target, controller, and light source, as illustrated in Fig.1.

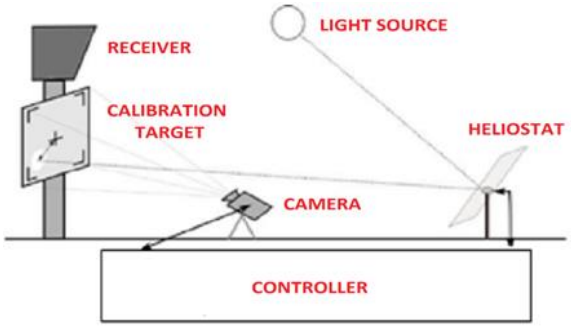

Fig.1. Prototype system layout.

The mechanical structure of the heliostat consists of the pedestal, heliostat facet, mirror, and rotary joints. All parts are installed to gather in many designs, each design takes care of varying the allowable azimuth and elevation heliostat angles. Also, may the design have less weight and more sustain to wind stresses or more resistance to mechanical fatigue.

The camera-based machine vision is used in heliostat calibration. High-resolution CCD camera is used to acquire images of the measurement target. The proposed technique is based on comparing the two-dimensional images of the target. The first image is one of the images that is acquired at certain azimuth and elevation angles, whereas the second image is the test image, which is needed to calibrate. These images are acquired from the camera at a certain position. Several target images for certain error cases are stored as bitmap images. Our initial trial is to compare the image under test with images of all errors that are previously acquired. The comparison is done by image matching that matches each pixel (x, y) in the image under test with the corresponding pixel (x, y) of the image of a certain error case. The mismatched pixels are counted and this process is repeated for all other error cases. This leads us to incorrect results in calibration.

To enhance the performance of our calibration technique, another comparing approach between two images is used El-Naggar et al.[14], which is measuring the Euclidean distance (De) of image features that describe the target. In this research work, pedestal tilt and deformation due to wind loading are selected. For each image, a set of seven invariant moments (φ_1, φ_2, φ_3, φ_4, φ_5, φ_6, φ_7) is computed as in Gonzalez and Woods [15].

First, the moment (m) of a 2-D image f (x, y) is computed as follows:

$$m_{pq} = \sum_x \sum_y x^p y^q f(x,y) \quad (1)$$

Where p, q =0, 1, 2, . . .

Then,the central moment (μ) is determined as a function of the previously computed moment as follows:

$$\mu_{pq} = \sum_x \sum_y (x - \bar{x})^p (y - \bar{y})^q f(x,y) \quad (2)$$

Where:

$$\bar{x} = \frac{m_{10}}{m_{00}} \quad (3)$$

and

$$\bar{y} = \frac{m_{01}}{m_{00}} \tag{4}$$

The normalized central moment (η) is then determined as a function of the central moment as follows:

$$\eta_{pq} = \frac{\mu_{pq}}{\mu_{00}^{\gamma}} \tag{5}$$

Where:

$$\gamma = \frac{(p+q+2)}{2} \tag{6}$$

Finally, the seven invariant moments (φ_i) as a function of the normalized central moment are computed, as in Gonzalez and Woods[15], as follows:

$$\varphi_1 = \eta_{20} + \eta_{02} \tag{7}$$

$$\varphi_2 = (\eta_{20} - \eta_{02})^2 + 4\eta_{11}^2 \tag{8}$$

$$\varphi_3 = (\eta_{30} - 3\eta_{12})^2 + (3\eta_{21} - \eta_{03})^2 \tag{9}$$

$$\varphi_4 = (\eta_{30} + \eta_{12})^2 + (\eta_{21} + \eta_{03})^2 \tag{10}$$

$$\varphi_5 = (\eta_{30} - 3\eta_{12})(\eta_{30} + \eta_{12})\left[(\eta_{30} + \eta_{12})^2 - 3(\eta_{21} + \eta_{03})^2\right] + (3\eta_{21} - \eta_{03})(\eta_{21} + \eta_{03})\left[3(\eta_{30} + \eta_{12})^2 - (\eta_{21} + \eta_{03})^2\right] \tag{11}$$

$$\varphi_6 = (\eta_{20} - \eta_{02})\left[(\eta_{30} + \eta_{12})^2 - (\eta_{21} + \eta_{03})^2\right] + 4\eta_{11}(\eta_{30} \mp \eta_{03}) \tag{12}$$

$$\varphi_7 = (3\eta_{21} - 3\eta_{03})(\eta_{30} + \eta_{12})\left[(\eta_{30} + \eta_{12})^2 - (\eta_{21} + \eta_{03})^2\right] - (\eta_{30} - 3\eta_{12})(\eta_{21} + \eta_{03})\left[3(\eta_{30} + \eta_{12})^2 - (\eta_{21} + \eta_{03})^2\right] \tag{13}$$

This set of moments is invariant or insensitive to translation, rotation, and scale change. These features are then stored for each error case. The Euclidean distance between the seven invariant moments for the case under test and all of the stored cases is computed as follows:

$$D_e = \sqrt{\sum_{i=1}^{7} (\varphi i_{undertest} - \varphi i_{errorcase})^2} \tag{14}$$

The minimum value of the total distances leads us to determine azimuth and elevation angles of the heliostat, regardless of the mechanical error that occurred. The controller used for tracking movement of the heliostat is shown in the block diagram in Fig.2.

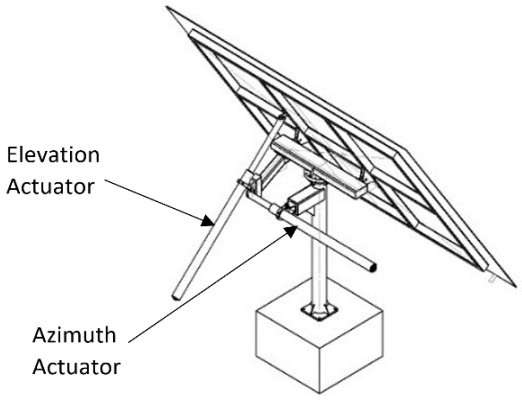

Fig.2. Linear actuator installation on the heliostat

3. THE EXPERIMENTAL SETUP

Heliostats are made up of, but not limited to, mechanical structure, foundations, mirrors, facets, and all the required associated fixings, components and infrastructure to ensure correct performance and operation in

all conditions. All these items have several design options and the final choice requires optimizing a combination of technical specifications and costs study. The present methodology is employed for the integrated design of a single facet small size heliostat with mirror area of 1 m^2, as shown in Fig.3.

Fig.3.Single faced small heliostat

In the linear drive system, the 1 m^2 mirror size allows for many solutions for the driven actuator, most of these solutions are referred to linear actuators. Power screw is one of the linear actuator types that become a trend to use in the CSP industry. The spread of this type is due to many advantages. It has a simple design, low cost, low duty cycle, easy installation, low maintenance, high wind withstands, and excellent precession. Fig. 4 shows the way the linear actuators are installed in the heliostat structure. However, in power screw, the hour angle limit is low compared to rotary actuators gives low azimuth and elevation tracking angles.

Fig.4 Linear actuator driven small sized heliostat 1m^2

4. THE EXPERIMENTAL RESULTS

Serval experiments have been conducted. Typical calibration digital records at noon of summer months for the adjustment of the elevation and azimuth angles of the heliostat are given in Table 1.

Table 1 Heliostat calibration angles change

Image	Heliostat elevation angle	Heliostat azimuth angle
A	45.38	198.64
B	45.43	199.258
C	45.386	199.966
D	45.471	199.966
E	45.529	201.162
F	45.619	201.8

Fig. 5 shows the reflected sun image on the target after the final installation of the heliostat. A remarkable deviation of the image centroid from the center of the target can be observed. This deviation has been recorded and compared with test image of the heliostat.

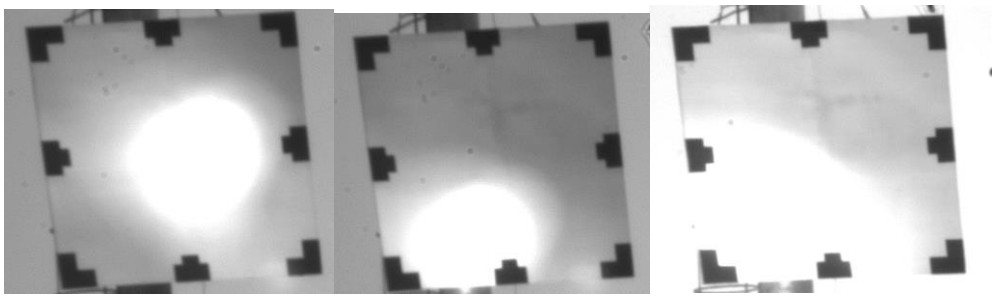

(A) (B) (C)

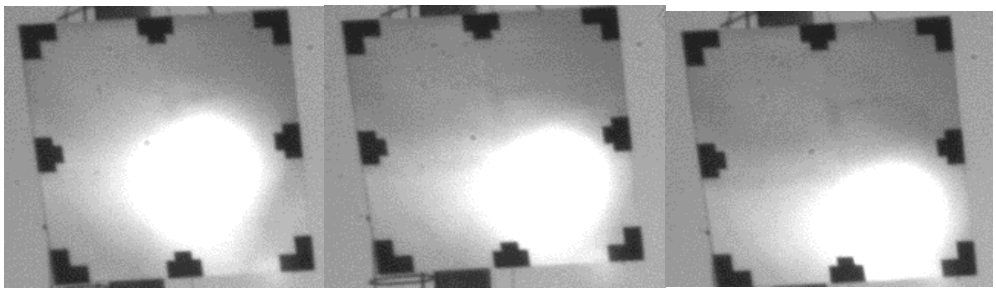

(D) (E) (F)

Fig. 5 The deviation of image centroid on heliostat

Table 2 shows the computed seven invariant moments (φ_1, φ_2, φ_3, φ_4, φ_5, φ_6, φ_7) of images A, B, C, D, E and F.

Table 2 The moment invariant of images A, B, C, D, E and F.

φ_i	Image A	Image B	Image C	Image D	Image E	Image F
φ_1	0.8096	1.3314	1.2901	1.2901	1.268	1.3385
φ_2	10.2462	37.0518	27.1831	27.183	28.0228	28.9587
φ_3	0.0290	0.1396	0.1444	0.1444	0.1417	0.1500
φ_4	0.0564	0.2706	0.2873	0.2873	0.2798	0.2953
φ_5	0.0009	0.0218	0.0246	0.0246	0.0233	0.0260
φ_6	0.1803	1.5724	1.4280	1.4280	1.1257	1.4286
φ_7	-0.0007	-0.0186	-0.0118	-0.0118	-0.0135	-0.0158

Table 3 shows the computed seven moments invariant (φ_1, φ_2, φ_3, φ_4, φ_5, φ_6, φ_7) of the test images A, B, C, D, E and F.

Table 3 The moment invariant of test images A, B, C, D, E and F.

φ_i	Test Image A	Test Image B	Test Image C	Test Image D	Test Image E	Test Image F
φ_1	0.7201	0.9941	1.3052	1.4142	1.2174	1.3268
φ_2	3.6922	29.7103	38.1558	12.0993	145.7934	28.7884
φ_3	0.0196	0.0627	0.0679	0.1566	0.1432	0.1486
φ_4	0.0394	0.1302	0.1286	0.3148	0.2832	0.2920
φ_5	0.0005	0.0051	0.0050	0.0295	0.0238	0.0254
φ_6	0.0725	-0.1766	-0.4476	1.0856	3.2802	1.3752
φ_7	-0.0000	0.0024	-0.0045	-0.0072	-0.0149	-0.0159

Table 4 shows the confusion matrix of the test images A, B, C, D, E and F after translation and scaling changes. For each image, there are 14 different positions introduced from different deterministic errors; e.g.; pedestal tilt, azimuth and elevation reference, deformation due to wind loading, non-level terrain, gear backlash, and back drive of the heliostat.

Table 4 The confusion matrix of the test images A, B, C, D, E and F.

	A	B	C	D	E	F
A	14	0	0	0	0	0
B	0	12	0	0	0	0
C	0	1	14	0	0	1
D	0	0	0	14	0	1
E	0	1	0	0	14	1
F	0	0	0	0	0	11

The computed true positive (TP) is 79 and the computed false negative (FN) is 5. The true positive rate (TPR) or recall is computed as in Tharwat[16] as follows:

$$recall = \frac{TP}{TP + FN} \quad (15)$$

The computed recall is 0.94.The false negative rate (FNR) is computed as inTharwat[16]as follows:

$$FNR = 1 - TPR \quad (16)$$

The computed FNR is 0.06. The computedoverall recognition rate is 94.0476 %.

5. CONCLUSION

The present study reported on the design and implementation of low-cost calibration system for single facet small heliostats using image analyses. The proposed system is based on moment invariant computations. The moment invariant features are insensitive to translation, rotation and scaling. The proposed system achieves accurate calibration results. The obtained FN is 5 and TP is 79. The achieved TPR is 0.94 and FNR is 0.06. The achieved recognition accuracy is 94.0476 %. As a future work, this work can be extended to diagnoses non deterministic errors.

References

[1]I. Reda and A.Andreas, “Solar Position Algorithm for Solar Radiation Applications”, National Renewable Energy Laboratory (NREL), Technical Report, January 2008.

[2] A. Pfahl, J. Coventry, M. Röger, F. Wolfertstetter, J. F. Vásquez-Arango, F. Gross, M. Arjomandi, P. Schwarzbözl, M. Geiger, and P. Liedke, “Progress in Heliostat Development”, Solar Energy, Vol. 152, pp. 3-37, August 2017.

[3] J. Masters, “Tower-Tracking Heliostat Array”, Faculty of California Polytechnic State University, March 2011.

[4] G. Bern, P.Schöttl, A.Heimsath and P. Nitz, “Novel Imaging Closed Loop Control Strategy for Heliostats” AIP Conference Proceedings, Vol. 1850, June 2017.

[5] M.Burisch, M. Sanchez, A.Olarra, and C. Villasante, “Heliostat calibration usingattached cameras and artificial targets”, AIP Conference Proceedings, Vol. 1734, May 2016.

[6] J.Terrés-Nícoli, C.Mansb and J.King, “Dynamic Effects of a Heliostat to Wind Loading”, Energy Procedia, Elsevier, Vol. 49, pp 1728-1736, 2014.

[7] M. Zavodnya, M. Slackb, R. Huibregtsec, A. Sonnd, “Tower-based CSP Artificial Light Calibration System”, Energy Procedia, Elsevier, Vol. 69, pp. 1488-1497, May 2015.

[8] J. Freeman, E. Kiranlal and S.Rajasree, “Study of the Errors Influencing Heliostats for Calibration and Control System Design”, IEEE International Conference on Recent Advances and Innovations in Engineering (ICRAIE-2014), May 09-11, 2014.

[9]G. Younkin, W. McGlasson, and R. Lorenz, “Considerations for low-inertia AC drives in machine tool axis servo applications,” IEEE Trans. on Ind. Appl. Vol 27, No 2, pp. 262-268, March/April 1991.

[10]M. Ebrahimi, " Analysis, modeling and simulation of stiffness in machine tool drives," omput Ind Eng, p. 38:93–105, 2000.

[11]J. Ziegler, "Optimum setting for automatic controllers," Trans ASME, p. 64:759–68, 1942.

[12]Y. Koren, " Control of machine tools," Trans ASME J ManufSciEng , p. 199:749–55, 1997.

[13]J. Freeman, " Novel ANFIS Based Control for Solar Energy Heliostats," Applied Mechanics & Materials, pp. 395-400, Vol. 704, 2014.

[14] M. El-Naggar, A. Hamdy, S. Moussa, and E. Shehab-El-Din, “A novel approach for fault diagnosis of power transformers based on extracting invariant moments”, Power Engineering Conference. AUPEC '08. Australasian Universities, 2008.

[15] R.Gonzalez and R.Woods, “Digital image processing”, 3rd Edition, Prentice Hall, Upper Saddle River, 2008.

[16] A. Tharwat, "Classification assessment methods", Applied Computing and Informatics,2020.